Error analysis and reliability of zero-order Lamb mode inversion for waveguide characterization

Sabbadini, A.; Massaad, J.; van Neer, P. L.M.J.; de Jong, N.; Verweij, M. D.

DOI
10.1016/j.ultras.2022.106703

Publication date
2022

Document Version
Final published version

Published in
Ultrasonics

Citation (APA)
Sabbadini, A., Massaad, J., van Neer, P. L. M. J., de Jong, N., & Verweij, M. D. (2022). Error analysis and reliability of zero-order Lamb mode inversion for waveguide characterization. *Ultrasonics*, *123*, Article 106703. https://doi.org/10.1016/j.ultras.2022.106703

Ultrasonics 123 (2022) 106703

Contents lists available at ScienceDirect

Ultrasonics

journal homepage: www.elsevier.com/locate/ultras

Error analysis and reliability of zero-order Lamb mode inversion for waveguide characterization

A. Sabbadini [a,*], J. Massaad [a], P.L.M.J. van Neer [a,b], N. de Jong [a,c], M.D. Verweij [a,c]

[a] Applied Sciences, Delft University of Technology, Lorentzweg 1, Delft, 2628 CJ, The Netherlands
[b] Ultrasone Lab, TNO, Oude Waalsdorperweg 63, Den Haag, 2597 AK, The Netherlands
[c] Biomedical Engineering, Department of Cardiology, Erasmus MC, University Medical Center Rotterdam, Doctor Molewaterplein 40, Rotterdam, 3015 GD, The Netherlands

ARTICLE INFO

Keywords:
Lamb wave
Multi-parameter inversion
Non-destructive testing
Sensitivity

ABSTRACT

In recent years, several fitting techniques have been presented to reconstruct the parameters of a plate from its Lamb wave dispersion curves. Published studies show that these techniques can yield high accuracy results and have the potential of reconstructing several parameters at once. The precision with which parameters can be reconstructed by inverting Lamb wave dispersion curves, however, remains an open question of fundamental importance to many applications. In this work, we introduce a method of analyzing dispersion curves that yields quantitative information on the precision with which the parameters can be extracted. In our method, rather than employing error minimization algorithms, we compare a target dispersion curve to a database of theoretical ones that covers a given parameter space. By calculating a measure of dissimilarity (error) for every point in the parameter space, we reconstruct the distribution of the error in that space, beside the location of its minimum. We then introduce dimensionless quantities that describe the distribution of this error, thus yielding information about the spread of similar curves in the parameter space. We demonstrate our approach by considering both idealized and realistic scenarios, analyzing the dispersion curves obtained numerically for a plate and experimentally for a pipe. Our results show that the precision with which each parameter is reconstructed depends on the mode used, as well as the frequency range in which it is considered.

1. Introduction

In a variety of fields, from medical research to industrial applications, measurements of the propagation of a mechanical wave through a medium are used to reconstruct its structure and material properties [1–9]. In the simple case of a fluid bulk medium, the propagation speed of a wave is proportional to the inverse square root of the density and the compressibility of the medium. However, when the object under investigation is a solid plate or a plate-like geometry, waves are characterized by sets of symmetric and antisymmetric dispersive wave modes. Waves characterized by these modes are referred to as Lamb waves [10]. The propagation speed of these wave modes depends not only on the elastic properties of the medium, but also on the product of its thickness and the frequency of the wave [10,11]. Thanks to their low attenuation and their sensitivity to shape variations, Lamb waves have been the object of intense research in the fields of non-destructive testing and defect detections [12–20]

Due to the dispersive behavior of Lamb waves, time-of-flight measurements of wave speed cannot be employed directly to reconstruct the properties of a medium [21,22]. Rather, a common approach consists in assuming that a given combination of shear speed (c_T), compressional speed (c_L) and thickness (h) defines uniquely a set of dispersion curves; based on this assumption, these three parameters can be reconstructed by extracting the dispersion curves from a measurement and then finding the parameters that generate the same (or most similar) curves [23–30]. Several techniques have already been developed to extract the dispersion curves from measured data and to solve the so-called inverse problem for one or more parameters simultaneously [24,28,29,31–35]. In most of these studies, the accuracy of the techniques is then compared with benchmarking methods, such as mechanical testing or pulse-echo measurements. However, little to no information is available on the reliability of the Lamb dispersion curve approach: whether the solution is unique and independent of the inversion algorithm employed, how robust this approach is with respect to noise, how sensitive different modes are to the three parameters and whether this sensitivity depends on the frequency range available, and, in general, how precise the results are. This information, however,

* Corresponding author.
E-mail address: a.sabbadini@tudelft.nl (A. Sabbadini).

https://doi.org/10.1016/j.ultras.2022.106703
Received 17 February 2021; Received in revised form 14 December 2021; Accepted 3 February 2022
Available online 19 February 2022

is crucial to assess whether and when this approach can be used in practical applications. If, for instance, two different sets of material properties generated similar A0 curves, and if noise would cause these curves to become indistinguishable, the inversion would not necessarily be able to distinguish between the two sets in practice.

In the first part of this work we present our approach to simultaneously extract c_T, c_L and h from measured or simulated dispersion curves. In addition to parameter extraction, the data extracted by our approach can be analyzed to retrieve quantitative information on how sensitive a mode is to each of the three parameters, as well as an indication of whether a solution is at least locally unique. We then employ this method to show numerically how random noise applied to the dispersion curves in the wavenumber direction can affect the results. Moreover, we show how the sensitivity of the zeroth order wave modes (A0 and S0) to variations of c_T, c_L and h changes between modes and how it depends on the frequency range available. Finally, we employ our approach for the analysis of experimental and simulated data, demonstrating its relevance for realistic applications (e.g. pipe measurements) as well as for the more idealized, numerical cases.

2. Setup

2.1. Numerical setup

The Finite Element software package PZFlex (Onscale, Redwood City, CA, USA) was used to run 2D simulations of the acoustic wave propagation of Lamb waves in a $h = 1$ mm thick stainless steel plate, which was simulated using nominal values of $c_L = 5800$ m/s, $c_T = 3100$ m/s and density $\rho = 7900$ kg/m^3. Damping was included by employing the Zener model built-in in PZFlex (a Kelvin–Voigt viscoelastic model in series with a linear spring), resulting in a linear damping of 0.3 dB/cm per MHz. Guided waves were excited in the plate by placing a small transducer on one of the surfaces and exciting it with a broadband ultrasound pulse with a center frequency of 2.7 MHz. Considering the lowest sound speed of the geometry, a mesh consisting of square grids with a length of 30 points per wavelength was defined to properly sample the guided waves. Along one of the surfaces of the plate, virtual receivers were placed every 0.1 mm over a distance of 90 mm, to record the time signals of these waves. Finally, a 2D Fast Fourier Transform (FFT) was applied to visualize the propagating wave modes, i.e. the dispersion curves, in the f–k_x domain.

2.2. Experimental setup

The experiments were conducted on a 40 mm -inner diameter 304-stainless steel pipe (nominal values: $c_L = 5920$ m/s and $c_T = 3141$ m/s, density $\rho = 8000$ kg/m^3) with a wall thickness of $h = 1$ mm. Due to the large diameter compared to the wavelength of the guided waves considered, the propagation modes are expected to be comparable to those one would observe in a stainless steel plate with the same thickness [36]. Two ATL P4-1 probes (Philips, Bothell, WA, USA), one functioning as an ultrasound source and the other as a receiver, were placed in line on the pipe wall (see Fig. 1), with a center-to-center distance of 10 cm, and were driven with a Verasonics Vantage 256 (Verasonics Inc., Kirkland, WA, USA) system. Each probe had a total of 96 elements with a pitch of 0.295 mm, corresponding to a total aperture of ≈ 28.32 mm. A 1-cycle pulse with a center frequency of 2.25 MHz was used to excite one element of the source probe, and all 96 elements of the receiver probe were used to record the propagating guided waves.

3. Methods

3.1. Dispersion curve extraction

Measured data

As can be seen in Fig. 3, the data recorded experimentally presents a large number of side-lobes around the dispersion modes. These are likely windowing artifacts connected to the aperture of the probe. In principle, it could be possible to reduce these artifacts by applying a spatially-tapered window to the recorded data, but this would increase the width of the main lobes (i.e. the dispersion curves), with the risk of resulting in overlapping modes. Rather than optimizing the aperture-windowing trade-off, which would be beyond the goal of this work, we adapted the following processing technique from [35] to isolate and extract the A0 and S0 modes (see Fig. 2). First, all the local maxima of the f–k_x surface were found and connected by straight lines, so as to generate a new, smoother dataset. This interpolation removes the valleys between consecutive peaks, e.g. turning a sawtooth pattern into a straight line. The new dataset, converted to decibel scale, was then squared (to increase the prominence of the highest peaks) and thresholded (to remove the lower values), thus partially isolating the modes and removing noise. The local maxima of the treated data were then extracted again and stored into a database (e.g. "$data_A$").

The mode identification was then executed as a search for chains of neighboring maxima: starting from a point in $data_A$, it was determined which (if any) other local maximum was the closest neighbor within a given radius; if such a point was found, the starting point would be moved from $data_A$ into a different database (e.g. "$mode_1$"), and the neighbor would become the next starting point. Once no neighbor was found within the searching radius, a new starting point was chosen from dataA and a new database (e.g. "$mode_2$") was created to store the next chain. Finally, spurious chains were separated from the real modes on the basis of chain length because a mode, being a set of points ordered along a curve, forms a consistently longer chain than randomly distributed spurious clusters of maxima). The modes themselves were identified on the basis of the order of appearance along the k_x direction: at every frequency, the k_x belonging to the A0 mode have a higher value than those belonging to the S0 mode.

Simulated data

The extraction of dispersion curves from the simulated data was more straightforward, thanks to the comparatively low level of noise and absence of windowing-related artefacts: the curves were found by extracting directly the local maxima in the untreated f–k_x domain, and were then sorted out according to the last step of the procedure described above. The results of the curve extraction algorithms are shown for both experiment and simulation in Fig. 3.

3.2. Curve fitting and error volumes

Once an experimental or simulated curve has been extracted, a fitting procedure can be used to identify the set of c_T, c_L and h (shear bulk wave speed, compressional bulk wave speed and thickness) that generates a theoretical curve that best matches the extracted ones. Typically, such fitting procedures consist in defining an error function that describes the discrepancy between the target and the model, and then applying an optimization algorithm to minimize this error. For instance, a least squares fitting algorithm can be used [24,32].

In contrast with other studies, the present work does not make use of an optimization algorithm to find the best fitting curve. Instead, a 3D parameter space of $c_T \in$ [2000–4000] m/s, $c_L \in$ [4500–7500] m/s and $h \in$ [0.1–4.0] mm was considered, with speed resolution of 50 m/s and thickness resolution of 0.1 mm. For each point in this space the theoretical curves of A0 and S0 were computed at frequencies comprised between 50 kHz and 3.6 MHz, sampled every 50 kHz. Each curve was then stored in a database. Similarly to other fitting procedures, an

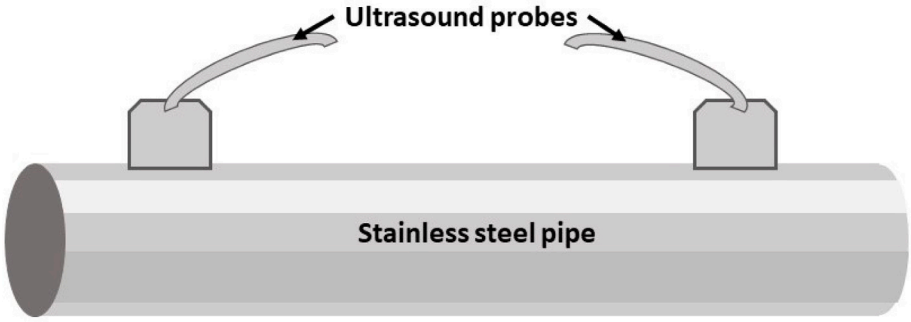

Fig. 1. Experimental setup, consisting of two ATL P4-1 probes held in contact with a 1 mm thick stainless steel pipe.

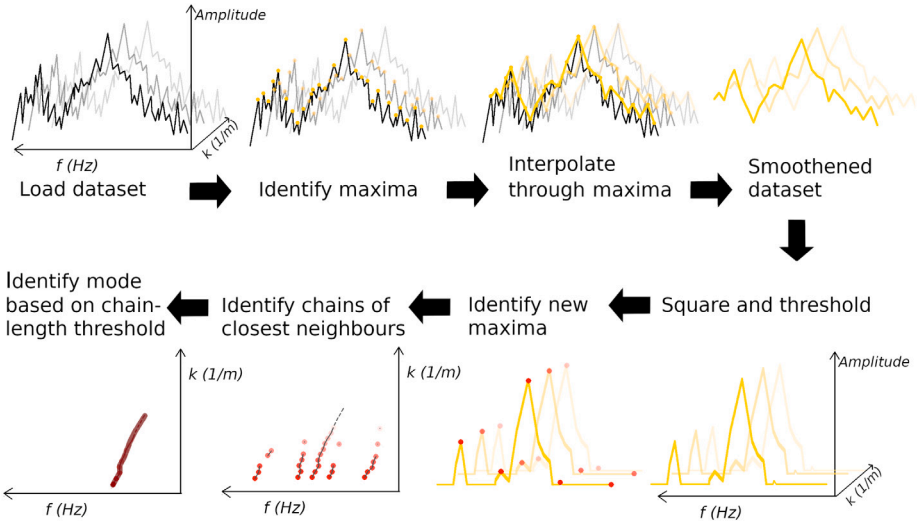

Fig. 2. Algorithm to extract the dispersion curves from experimental data in the frequency–wavenumber domain.

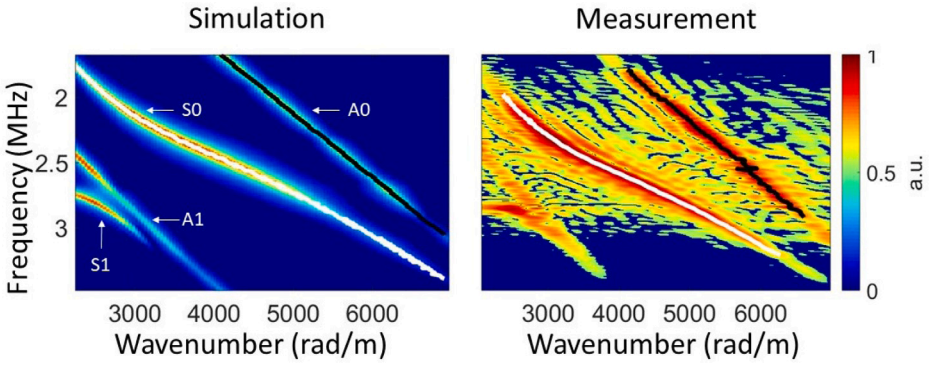

Fig. 3. Magnitude of a 2D FFT applied to time signals obtained on the surface of a 1 mm-thick simulated stainless steel plate (left) and measured on the surface of a 1 mm-thick stainless steel pipe (right). The white lines show the reconstructed S0 curve, the black lines indicate the reconstructed A0 mode.

error function E was then introduced, defined here as a Mean Absolute Percentage Error (MAPE),

$$E = \frac{100}{N} \sum_{i}^{N} |k_i^{Th} - k_i| / k_i^{Th} \tag{1}$$

where N is the number of frequencies considered, the index i runs from 1 to N, k_i is the wavenumber corresponding to the ith frequency of the measured dispersion curve, and k_i^{Th} is the wavenumber of the theoretical curve at the same frequency.

The extracted curves were compared to every theoretical curve in the corresponding database, and the MAPE of each comparison was added to a 3D plot. The resulting image shows the volumetric distribution of the MAPE in the entire parameter space. We will refer to this distribution as "error volume". Once the error volume has been reconstructed, it is possible to identify the best fitting theoretical curve by finding the coordinates of the global minimum of the MAPE. Moreover, this approach allows one to observe the distribution of the error in the parameter space.

3.3. Fitting reliability

To study how noise can affect the correct identification of c_T, c_L and h, we employed as target curves the theoretical dispersion curves of the A0 and S0 modes, thus excluding the influence of other factors

(e.g. experimental artifacts, discretization-related errors) on the final result. The theoretical curves were calculated by solving numerically the Lamb equations [11] using a built-in zero-crossing search algorithm of Matlab (version r2018b, MathWorks, Natick, MA, U.S.A.). Random noise was then assigned to the wavenumber coordinate of each point on the curves. At each point, the noise applied was drawn from a uniform distribution of values between −0.5% and 0.5% of the wavenumber value of the point. The boundaries of the noise distribution were chosen so that the minimum MAPE would be comparable to that of the simulated data, lying between 0.2% and 0.4%, the observed the global minimum MAPE of the simulated A0 and S0, respectively. Repeating the analysis for ten different realizations of the noise, we observed that the minimum MAPE value could vary by up to approximately 0.1 times its average value.

Within the resolution of the database, it is possible to determine whether the minimum is global, as well as how sensitive the error is to the different parameters. For instance, if many points along the c_L axis correspond to comparably low values of MAPE, similar curves can be generated by different values of compressional speed; the optimal value of c_L may therefore be not reliable.

A traditional sensitivity analysis would be ill suited to describe the reliability of MAPE minimizations, due to its local nature (see Appendix). Instead, to quantify this concept of reliability based on the error volume analysis, we introduce two parameters: a low error volume (LEV) and a spread around the minimum (SAM). The LEV value indicates the number of theoretical curves whose MAPE is at most 1.1 times the global minimum; this boundary was chosen based on the factor 0.1 variation in minimum MAPE that was observed to come from random noise. Notably, the points within the LEV form a curved shape within the 3D space, thus the LEV cannot be described as a rectangular volume (i.e. as the product of three orthogonal coordinates). The SAM values indicate how far away from the minimum the other low error points are spread, along each axis. The SAM values are computed as a weighted mean absolute percentage deviation from the coordinates with minimum MAPE:

$$SAM_X = \frac{100}{i_{min_X}} \sum_{i \in LEV} \frac{|i_X - i_{min_X}|}{E_i - E_{min}} \left(\sum_i \frac{1}{E_i - E_{min}} \right)^{-1} \quad (2)$$

where SAM_X is the SAM value along the X axis (e.g. compressional speed), $\boldsymbol{i}(X,Y,Z) = (i_X, i_Y, i_Z)$ is a point within the LEV, i_X is the X coordinate of the $\boldsymbol{i}$ point, E_i is its corresponding MAPE, i_{min_X} is the X coordinate of the point with minimum MAPE, E_{min} is the minimum value of MAPE, and the sum runs over all the points $\boldsymbol{i} \in LEV$, excluding the global minimum (the point with minimum MAPE). This function was chosen so as to give more relevance to the points whose MAPE is the most similar to the minimum. The percentage term $100/i_{min_X}$ was included to allow the comparison of SAM values of different axes.

4. Results

4.1. Error volumes

Simulated data

Fig. 4 shows slices of the error volume computed for an A0 curve extracted between 1.5 and 3.1 MHz from simulated data. A global minimum exists within the parameter space considered, and corresponds to a MAPE of 0.218% at coordinates $c_L = 4800 \pm 25$ m/s, $c_T = 3200 \pm 25$ m/s, and $h = 1.1 \pm 0.05$ mm. The indicated variations are due to the step-sizes of the parameters. The material properties corresponding to the best fitting curve, therefore, are in poor agreement with the actual values $c_L = 5800$ m/s, $c_T = 3100$ m/s and $h = 1$ mm. As can be seen in the plot, however, there is an extended volume in the parameter space in which the MAPE is within 1%. In fact, the third-lowest error point corresponds to a MAPE of 0.225% at coordinates: $c_L = 5850 \pm 25$ m/s, $c_T = 3100 \pm 25$ m/s, and $h = 1.0 \pm 0.05$ mm, which are in much better agreement with the input parameters of the simulation.

Table 1
Values of LEV and SAM for the A0 and S0 modes extracted from a simulated 1 mm thick stainless steel plate (above) and from an experiment on a 1 mm thick stainless steel pipe (below) at frequencies between 1.5 MHz and 3.1 MHz.

Simulated data 1 mm thick stainless steel plate				
Mode	LEV	SAM_{c_L}	SAM_{c_T}	SAM_h
A0	50	20.8%	3.2%	10.0%
S0	14	0.8%	0.0%	0.0%
Experimental data 1 mm thick stainless steel pipe				
Mode	LEV	SAM_{c_L}	SAM_{c_T}	SAM_h
A0	209	13.0%	2.1%	7.0%
S0	7	3.8%	0.4%	0.0%

The same analysis was performed for the S0 mode extracted from the simulated data, see Fig. 5. Once again, there is a global minimum error within the parameter space, corresponding to a MAPE of 0.551% at coordinates $c_L = 5850 \pm 25$ m/s, $c_T = 3100 \pm 25$ m/s, and $h = 1.0 \pm 0.05$ mm. As can be seen in Fig. 5, the distribution on the c_L–c_T plane is similar to that of the A0 mode, while the distribution on the other planes is clearly different. Interestingly, while the coordinates of the global minimum are much closer to the expected values than those of A0, overall the MAPE is higher. This result suggests that, at the frequencies considered, variations in the parameter space of material properties causes greater variations in S0 than in A0 curves. As a consequence, an extracted S0 curve that deviates more from the theoretical one may still yield parameters that are closer to the actual ones, as compared to the A0 case.

Comparing the A0 and S0 error volumes, we can observe that they show a similar trend for the distribution of the low errors along the compressional speed axis (almost uniform for $c_L > 5000$ m/s, indicating a low sensitivity to overestimations of this parameter), whereas the distribution in the c_S–h plane is different: for the S0 mode, the coordinates of low error points on the c_S axis increase with increasing thickness, while for the A0 mode the distribution along h is similar to that along c_L, indicating low sensitivity to thickness overestimations.

Measured data

Figs. 6 and 7 show the error volumes computed for the A0 and S0 curves extracted from the experiment. Qualitatively speaking, the volumes appear very similar to those of the simulated data. The material properties identified by the minimum of the error volume of A0 are $c_L = 5500 \pm 25$ m/s, $c_T = 3100 \pm 25$ m/s, and $h = 1.0 \pm 0.05$ mm; those extracted from S0 are $c_L = 5250 \pm 25$ m/s, $c_T = 3250 \pm 25$ m/s, and $h = 1.0 \pm 0.05$ mm.

Subsequently, the LEV and SAM values were computed for the two modes for both simulated and experimental data, and are reported in Table 1. For each dataset, the S0 mode appears more sensitive than the A0: the LEV and all the SAM values are smaller, confirming that variations in the parameter space of material properties lead to greater variations in S0 than in A0.

4.2. Robustness against noise

The theoretical curves of A0 and S0 were calculated between 50 KHz and 3.5 MHz for a 1 mm thick stainless steel plate. As described in Section 2.3, random noise was added to the wavenumber coordinates of both curves. For each curve, the error volume was reconstructed and used to identify the best fitting curve, i.e. the curve with minimum error . This procedure was repeated ten times for each mode. Table 2 shows the average and highest minimum MAPE, and the mean absolute error (MAE) and maximum error of c_T, c_L and h, compared to their true values ($c_L = 5800$ m/s, $c_T = 3100$ m/s, and $h = 1.0$ mm), for each mode.

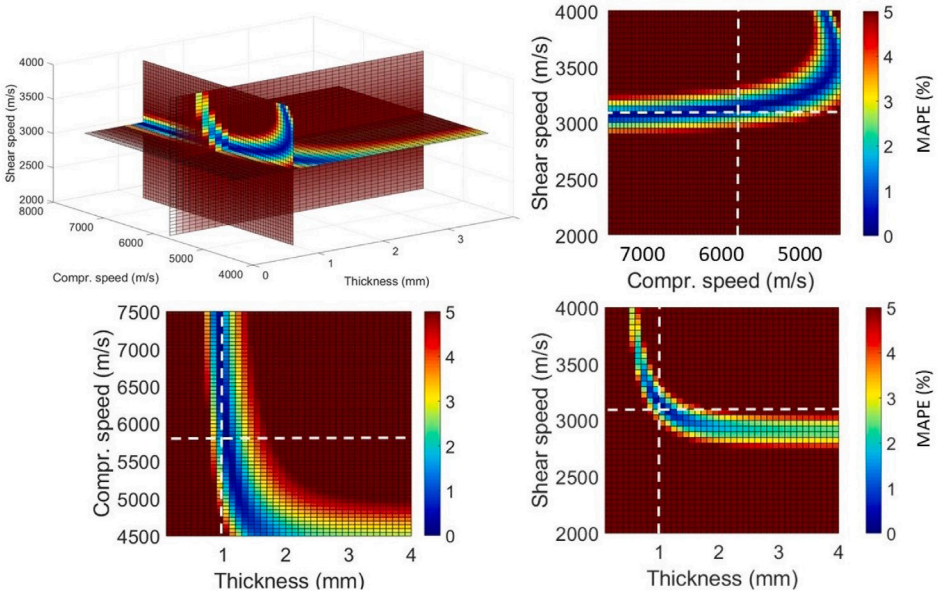

Fig. 4. The top-left panel shows slices of the error volume for the simulated A0 mode of a stainless steel plate at frequencies between 1.5 and 3.1 MHz . The slices represent planes at the fixed values $c_L = 5800$ m/s, $c_T = 3100$ m/s, and $h = 1$ mm, which are the actual values of these parameters . Each other panel shows the frontal view of a single plane (c_L–c_T, c_T–h, c_L–h, in clockwise order). Colors represent the value of MAPE at each coordinate in the parameter space. The white dashed lines show where the planes intersect in each view.

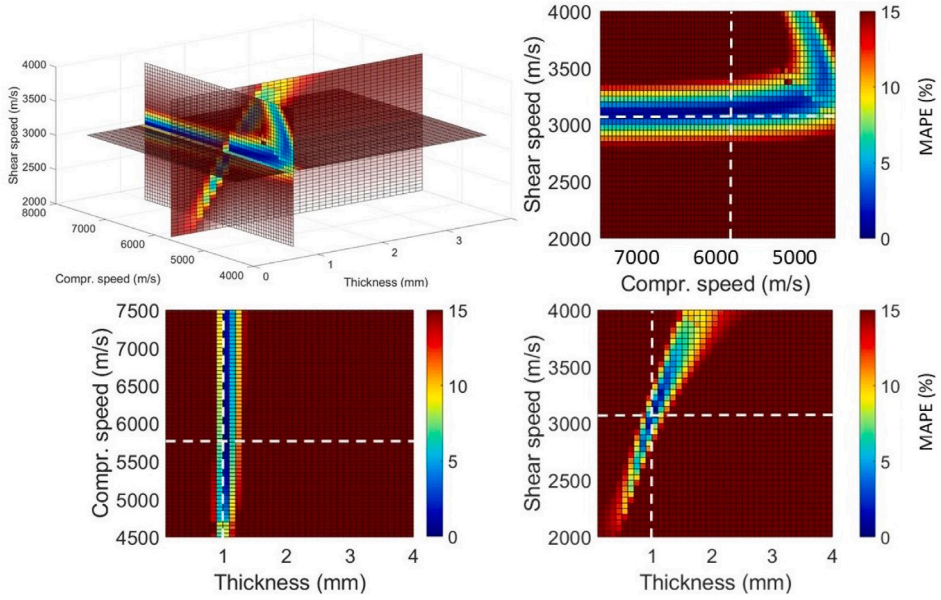

Fig. 5. The top-left panel shows slices of the error volume for the simulated S0 mode of a stainless steel plate at frequencies between 1.5 and 3.1 MHz . The slices represent planes at the fixed values $c_L = 5800$ m/s, $c_T = 3100$ m/s, and $h = 1$ mm, which are the actual values of these parameters . Each other panel shows the frontal view of a single plane (c_L–c_T, c_T–h, c_L–h, in clockwise order). Colors represent the value of MAPE at each coordinate in the parameter space. The white dashed lines show where the planes intersect in each view.

Table 2
Results of generating ten A0 and ten S0 curves affected by uniformly distributed random noise applied to the wavenumber coordinates. Entries in the table show, from left to right: the average minimum MAPE ($\bar{E}$), the highest value of minimum MAPE (E_m), the mean and maximum absolute error of c_L compared to the true value (MAE c_L and $\Delta c_{L_{max}}$), the mean and maximum absolute error of c_T compared to the true value (MAE c_T and $\Delta c_{T_{max}}$), and the mean and maximum absolute error of h compared to the true value (MAE h and Δh_{max}.

Mode	$\bar{E}$ (%)	E_m (%)	MAE c_L (m/s)	$\Delta c_{L_{max}}$ (m/s)	MAE c_T (m/s)	$\Delta c_{T_{max}}$ (m/s)	MAE h (mm)	Δh_{max} (mm)
A0	0.25	0.27	95	1000	10	100	0.01	0.1
S0	0.24	0.26	5	50	0	0	0.00	0.0

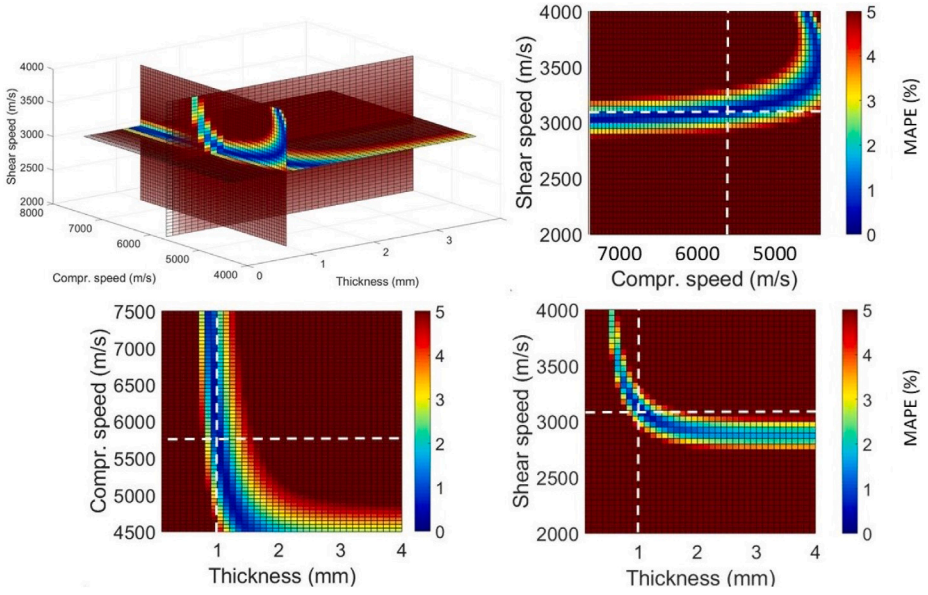

Fig. 6. The top-left panel shows slices of the error volume for the A0 mode extracted from an experiment on a 1 mm thick stainless steel pipe at frequencies between 1.5 and 3.1 MHz . The slices represent planes at the fixed values $c_L = 5800$ m/s, $c_T = 3100$ m/s, and $h = 1$ mm, which are the actual values of these parameters . Each other panel shows the frontal view of a single plane (c_L–c_T, c_T–h, c_L–h, in clockwise order). Colors represent the value of MAPE at each coordinate in the parameter space. The white dashed lines show where the planes intersect in each view.

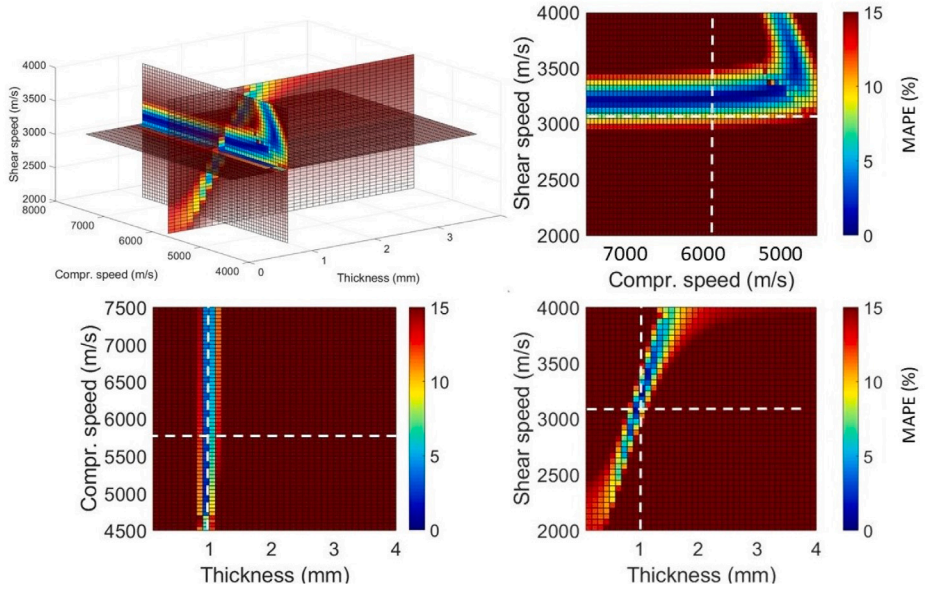

Fig. 7. The top-left panel shows slices of the error volume for the S0 mode extracted from an experiment on a 1 mm thick stainless steel pipe at frequencies between 1.5 and 3.1 MHz . The slices represent planes at the fixed values $c_L = 5800$ m/s, $c_T = 3100$ m/s, and $h = 1$ mm, which are the actual values of these parameters . Each other panel shows the frontal view of a single plane (c_L–c_T, c_T–h, c_L–h, in clockwise order). Colors represent the value of MAPE at each coordinate in the parameter space. The white dashed lines show where the planes intersect in each view.

4.3. Frequency range analysis

During data analysis, we observed that theoretical curves generated for different values of one parameter could be more similar to each other at certain frequencies than at others. For example, the MAPE between two S0 curves corresponding to thicknesses of 1 mm and 1.2 mm, for shear and compressional speeds fixed at 3100 and 5800 m/s respectively, was less than 1% at frequencies between 0 and 1 MHz and around 18% between 1.5 and 2.5 MHz.

To investigate how different frequency regions affected the LEV and SAM results, comparison of noiseless theoretical A0 and S0 curves to the database was performed at various frequency ranges. The frequency ranges considered included bands with a width of 0.2 to 2.9 MHz, within an overall range of 0.1–3.1 MHz. For each frequency range, the LEV and SAM values were computed and plotted. For this calculation only, the LEV was defined as all the curves whose MAPE was within 110% of the second-lowest error, instead of the lowest error. This choice was made because the lowest error was always zero, since theoretical curves were considered and the database contained the theoretical curves themselves.

Figs. 8 and 9 show the values of LEV and SAM at different frequency ranges for the noiseless theoretical A0 and S0 curves, respectively, of a 1 mm thick stainless steel plate. The vertical axis represents the starting frequency for each of the ranges considered, while the horizontal axis represents the bandwidth of each range. Since only

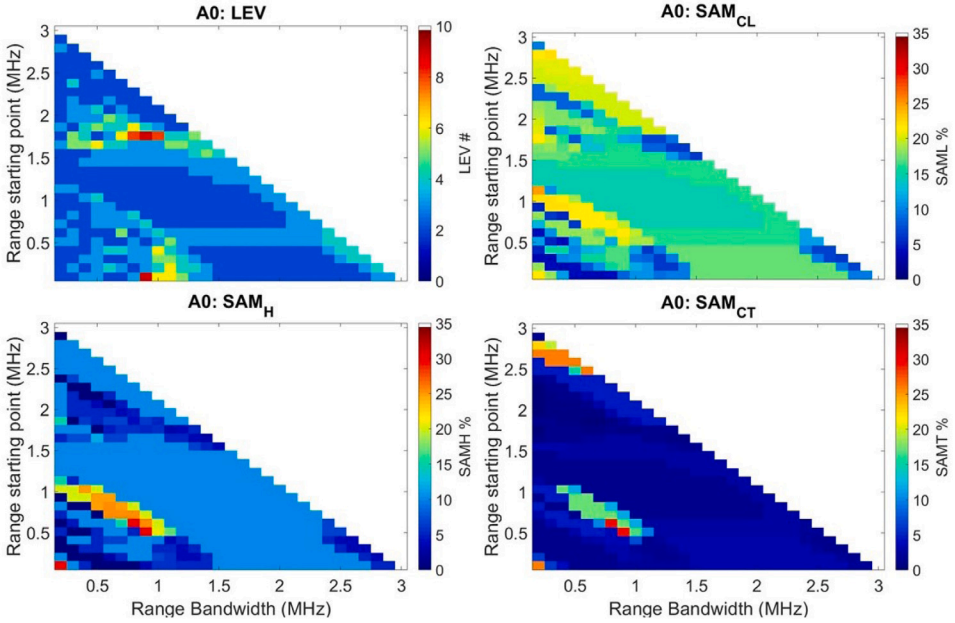

Fig. 8. LEV, SAM c_L, SAM c_T, and SAM h for a theoretical A0 curve at different frequency ranges. The colors represent the amplitude of each variable, with each point corresponding to a different combination of bandwidth and starting frequency.

frequencies between 0.1 and 3.1 MHz were considered in this analysis, the maximum bandwidth of the frequency ranges decreases with the increase of the starting frequency. Each point in the plots shown in Figs. 8 and 9 thus corresponds to an analysis performed at a different frequency range, determined as the combination of a starting frequency and a bandwidth.

For A0, considering only higher frequencies introduces a greater variability of compressional speeds within the LEV, while the highest precision seems to be achievable for all three parameters within the first MHz; the value of SAM of the shear speed appears to be relatively low (within 50 m/s) at most frequencies. The LEV itself can vary considerably depending on the frequency band considered. In contrast, the SAM values for the S0 mode are almost uniformly low at the higher frequencies, while there is a region of frequencies around 0.5 MHz in which they increase, especially for the thickness.

5. Discussion

Several studies can be found in literature detailing techniques to extract Lamb dispersion curves and inversion methods to reconstruct material properties [23,24,27–29,31–35,37,38]. However, these studies rely on minimization techniques that only yield information about the (possibly) global minimum of a given error function. When employing such an approach, therefore, all information about how the error is distributed over the parameter space is lost. One of the advantages of the comparison approach presented in this paper is that information about the matching error of the dispersion curves (the MAPE defined in Eq. (1)) is extracted along with the coordinates of the global minimum, at the cost of having to initially compute and store dispersion curves for the entire parameter space. This additional information is necessary to assess how reliable the results of the inversion are, both in a general sense (i.e. how precise can we expect a multi- or single-parameter inversion to be) and for a specific measurement (e.g. how reliable a measurement is performed with a given setup under specific experimental conditions and corresponding experimental noise). Moreover, our results identify which zeroth order wave mode is the most sensitive to what material property at what frequencies, and the approach we have presented here could also be employed to extend these results to higher order modes and higher frequencies, providing a toolset to maximize the precision of the results of inversion. Finally, while it may be possible to further improve the accuracy of the data acquisition and preprocessing (i.e. the dispersion mode extraction) steps, identifying the parameters of a sample with high accuracy was beyond the purpose of our work. We did, however, explore a range of accuracy of the target curve by considering different levels of idealization (from curves derived directly by the Lamb equations, to experimental data), showing the relevance of the information provided by our approach in all scenarios.

To better understand how information on the MAPE is connected to the precision of the inversion, let us consider the following: if, along a given axis (e.g. compressional wave speed), there are multiple coordinates at which the MAPE is comparable to the global minimum, then many curves corresponding to different material properties are comparably similar to the target one (e.g. the one extracted from experiments). Small variations in the target curve, for instance due to experimental noise or poor reconstruction of the wave mode, could then greatly shift the location of the global minimum and therefore the values of the reconstructed properties. Knowing the distribution of the MAPE, then, allows one to know how much the material properties can vary with small variations of this error. Intuitively, the larger the range of parameters with a low error, the less reliable are the properties corresponding to the global minimum.

To provide a quantitative measure of the sensitivity described above, we have introduced the values of Low Error Volume (LEV) and Spread Around Minimum (SAM). The LEV value represents how many different curves have a MAPE comparable to the minimum one. Here, ‘comparable’ is defined as a threshold of up to 10% higher than the minimum MAPE. By itself, however, the LEV is not sufficient to tell whether a result is reliable: if there were 100 curves represented within the LEV, but all located at similar coordinates, even if the global minimum was shifted to another point (e.g. due to noise), the result would not be affected greatly. The SAM values represent how the error spreads along each parameter axis: a lower spread along one axis means a higher precision with respect to the corresponding parameter. This is different from a standard sensitivity analysis, in that the SAM values consider all the points within the LEV to determine how much a coordinate could vary, whereas the sensitivity analysis only looks at the derivatives in the neighborhood of the minimum, fixing two coordinates out of three at a time. A more detailed explanation of why this local information is not sufficient is given in the Appendix.

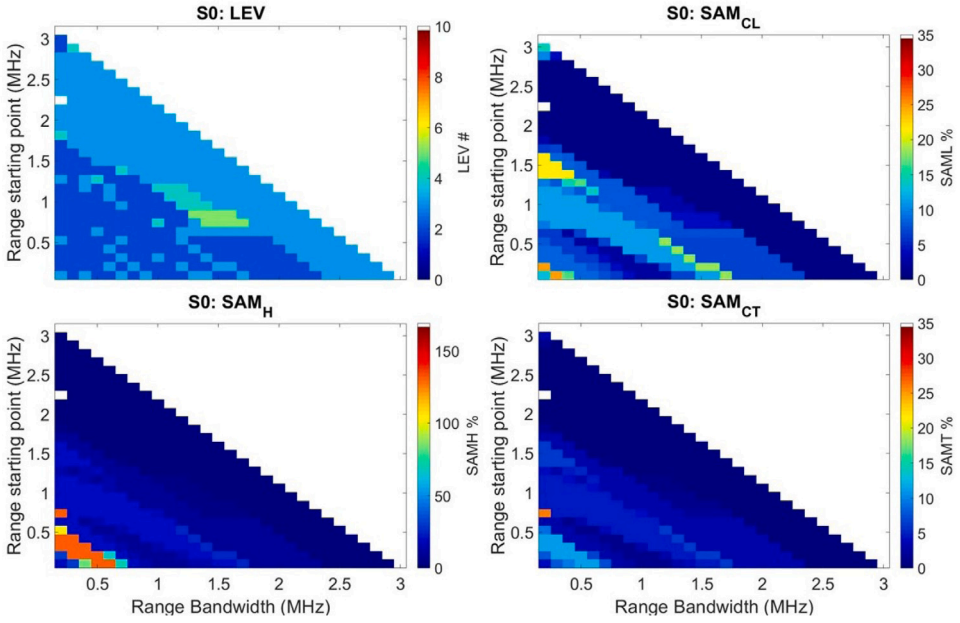

Fig. 9. LEV, SAM c_L, SAM c_T, and SAM h for a theoretical S0 curve at different frequency ranges. The colors represent the amplitude of each variable, with each point corresponding to a different combination of bandwidth and starting frequency.

Practical observations guided the choices made for the LEV and SAM thresholds: the LEV boundary (110% of the minimal MAPE) was established based on the observed variability in minimal MAPE when the target curve was a theoretical curve with uniformly distributed random noise on the wavenumber coordinates; the SAM values were computed as an average weighted by the inverse of the MAPE, to reflect that lower error curves are more likely to be mixed up with the curve of the global minimum. As long as LEV and SAM are defined consistently, they allow to compare different curves of the same wave mode, different wave modes and frequency ranges, and even different experiments.

By employing the LEV and SAM parameters, it was also possible to analyze how the sensitivity of the A0 and S0 modes varies with the frequency range over which the curves are compared. In particular, Figs. 8 and 9 show that the A0 mode can be more reliable than S0 in estimating the compressional wave speed and the thickness when only low frequencies are available, i.e. up 1 MHz for a 1 mm plate. At higher frequencies, the S0 mode appears to provide more precise information about all three parameters. Notably, in our study we have only focussed on zeroth order modes, and these two modes were only analyzed separately. As mentioned above, however, our approach can be used also to analyze higher order modes. It would be interesting to investigate, then, if combining multiple modes at their "best" frequency ranges, e.g. by combining their error volumes by sum or multiplication, could improve precision or accuracy.

Low values of LEV and SAM, however, do not guarantee that the minimum error curve corresponds to the true values of the properties of the medium; they should be interpreted as a measure of precision, rather than accuracy. In fact, when comparing the A0 and S0 modes in the experimental data, the SAM and LEV values are lower for S0, but the parameters identified by the minimum of the error volume of A0 are more accurate compared to the expected nominal properties of the pipe. This result means that, in this one measurement, the curves extracted from the experiment yield a more accurate result for A0 than for S0; however, given the higher values of SAM and LEV, it is reasonable to expect that repeated experiments would show a greater variation in results for A0 than for S0. It is also worth mentioning here that the central assumption of this paper, i.e. that we can use the Lamb characteristic equations to describe our measurements, is verified only in an approximate sense: the equations, in fact, are defined for infinite plates with perfectly parallel, smooth surfaces and elastic, homogeneous and isotropic materials, while a real metal plate necessarily presents surface roughness and imperfections, warping, and anisotropic behaviors due to sheet fabrication process. For finite element simulation, moreover, the applied discretization scheme (size and shape of the elements, interpolation between nodes) can alter the accuracy with which results are calculated. All of these factors are likely to cause deviations from the theoretical curves, and it is reasonable to expect that different modes will be affected differently, due to their different particle motion patterns and wave velocities.

Besides providing information on the distribution of the matching error, the approach we employ in this study has several other advantages over traditional optimization algorithms. For one, its results do not depend on initial guesses. Moreover, most of the computational cost lies in the generation of the database of theoretical curves that is used for the comparisons with the target curve; once the database exists, it can be used any number of times on any number of different experimental or simulated curves. In contrast, every time an optimization algorithm runs, it has to re-compute each theoretical curve it uses. While the number of curves thus computed is usually lower than that necessary to create a database, the cost for the database is paid only once, whereas that of the optimization is paid every time it is employed. In terms of real-world applications, this approach could benefit greatly the efficiency of in-situ non-destructive tests, such as pipe inspections, where the database could be computed during the fabrication of the testing instrument, ready to be used at every subsequent test.

A drawback of the database approach, however, is that it only provides results within its parameter space, which is defined at the moment of the creation of the database. Moreover, there is a trade-off between accuracy (limited by the resolution of the database), range of parameters explored (defined by the boundaries of the database) and size of the database itself (for reference, the database used in the present work has a size of 55 Mb). This problem can be circumvented by preparing various application-specific databases, in which resolution and boundaries of a database are tailored to the use it has to serve, e.g. analyzing a steel pipe with nominal thickness of 1 mm.

Finally, the results presented in Table 2 highlight a potential general weakness in the approach of inverting dispersion curves to reconstruct material properties. In fact, while the S0 curve showed less sensitivity to the random noise, one out of ten noise-affected A0 curves yielded

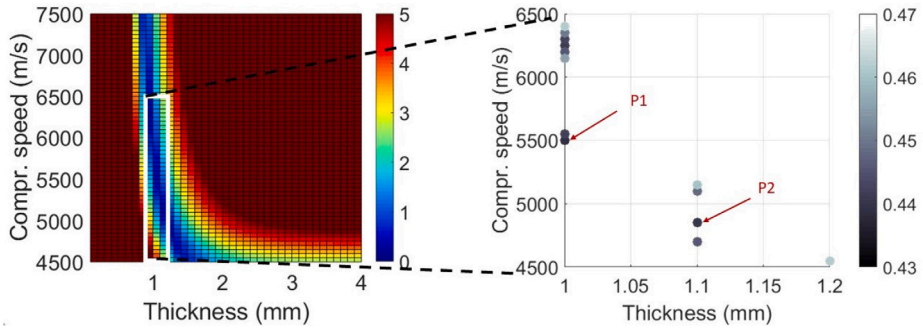

Fig. 10. Left panel: the h–c_L slice of Figure 5.6. Right panel: the LEV of this dataset, collapsed onto the h–c_L plane. Highlighted are P_1 and P_2, the points corresponding to the lowest and second-lowest values of MAPE, respectively. The colors in both panels represent the MAPE.

a compressional speed 1000 m/s lower than the true value. Repeating the same analysis with noise randomly distributed across a wider range (between −1% and 1% of each wavenumber coordinate), comparable to the average variations observed in the experiment, yielded three cases out of ten in which the compressional speed extracted from the A0 curve was between 800 and 1000 m/s lower than the true value. These results would suggest that the properties found by inverting the A0 curve can be considerably affected by noise, undermining their reliability in practical applications. Moreover, here all three parameters (shear and compressional wave speeds, and thickness) were extracted simultaneously, but it would also be reasonable to investigate whether prior knowledge on some of the parameters would improve the results. Indeed, for a noise-affected theoretical A0 curve in which three-parameters estimation yielded $c_L = 4800$ m/s, we observed that fixing the thickness at 1.0 mm corresponded to a minimum error curve generated by $c_L = 5500$ m/s; fixing both the thickness at 1.0 mm and the shear speed at 3100 m/s yielded an estimated $c_L = 5850$ m/s, suggesting that a priori knowledge of some parameters can increase the robustness of results against noise.

In principle, using our results, it could even be possible to extract a single property using the most precise combination of mode and frequency range, then use that property as input fixed value and extract the second property, again based on its corresponding best mode and frequency range, and iterate until all properties are extracted. This boot-strapping approach could be very useful in applications where a priori knowledge is not available; however, it remains to be proven whether it would have the same effect, which likely depends on the accuracy with which the first property is extracted. In any case, it would be interesting to perform a more extensive analysis, both on noise-affected theoretical curves as well as on repeated experiments, to determine what percentage of cases leads to significant over- or underestimations of material properties.

6. Conclusions

In this work we have presented a new approach for the analysis of Lamb dispersion curves for material characterization. In addition to parameter extraction, the data extracted by our approach can be analyzed to retrieve quantitative information on the precision with which the information is extracted. We have observed that low amplitude random noise can affect the results of Lamb wave dispersion curve inversion, with few A0 curves yielding compressional speeds far off their true value, thus highlighting the importance of having such a measure of precision. Moreover, using the proposed method, we have shown that the S0 mode is more sensitive than the A0 mode to all three properties at higher frequencies, and that both modes are more sensitive to shear speed and thickness than to compressional speed. These results could therefore be employed to increase the precision with which the material properties are reconstructed, by identifying the optimal combination of wave mode and frequency range for each.

Declaration of competing interest

The authors declare that they have no known competing financial interests or personal relationships that could have appeared to influence the work reported in this paper.

Acknowledgment

This work is part of the STW – Dutch Heart Foundation partnership program “Earlier recognition of cardiovascular diseases” with project number 14740, which is financed (in part) by The Netherlands Organization for Scientific Research (NWO).

Appendix. Sensitivity analysis

In the main text, we often refer to the reliability of extracting parameters by comparing dispersion curves of Lamb modes, or the sensitivity of such a procedure to each parameter. A well-known approach to quantify this information is to perform a so-called sensitivity analysis. In our case, this could be done by considering the error function E (corresponding to the MAPE values) and computing its first derivatives around the minimum. For example, the sensitivity of E with respect to variations on the compressional speed axis can be calculated as:

$$S(c_L, P) = (\partial E/\partial c_L)|_P \tag{3}$$

where S is the sensitivity, c_L is the compressional speed, and $|_P$ indicates that the derivative is evaluated at the coordinates (c_L^P, c_T^P, h^P) of the point P, which corresponds to the minimum MAPE value. This value of S expresses how fast the function E grows for small variations of the c_L coordinate. However, it does not provide any information on the existence and location of the local minima of comparable depth that can exist within the MAPE space. As such, the sensitivity analysis does not show that a small variation in MAPE could lead to large variations in e.g. c_L. The SAM and LEV values were introduced to provide this necessary information.

In Fig. 10, the left panel is the same as in Fig. 6, while the right panel shows all the points within the LEV, projected onto the h–c_L plane. The points highlighted as P_1 and P_2 in the right panel correspond to the minimum and second-minimum MAPE points, respectively. The coordinates of P_1 are: $c_L = 5500$ m/s; $c_T = 3100$ m/s; $h = 1.0$ mm; The coordinates of $P2$ are: $c_L = 4850$ m/s; $c_T = 3150$ m/s; $h = 1.1$ mm. The MAPE of P_1 is 0.439%, the MAPE of P_2 is 0.441%. These numbers show that the two curves corresponding to P_1 and P_2 are very similar to each other; the smallest alteration of P_1 could turn it into P_2, resulting in an extracted compressional speed of 4850 m/s instead of 5500 m/s.

The sensitivity analysis of E in the c_L direction around P_1, $S(c_L, P_1) = 0.5$ ms/m (i.e. the MAPE grows by approximately 6% in a step of 50 m/s on the c_L axis) is limited to a local description along

a single axis, and it does not provide any information to describe the situation shown in Fig. 5.10. The SAM c_L value of 604 m/s, on the other hand, accounts for the entire LEV (across all three axes), and it does show that small variations of the MAPE could potentially lead to large variations in compressional speed. As such, in this situation the LEV and SAM values are necessary to provide the quantitative description that a standard sensitivity analysis cannot supply.

References

[1] K. Heller, L.J. Jacobs, J. Qu, Characterization of adhesive bond properties using {L}amb waves, NDT E Int. 33 (8) (2000) 555–563.

[2] Christine Valle, Jerrol W. Littles, Flaw localization using the reassigned spectrogram on laser-generated and detected lamb modes, Ultrasonics 39 (8) (2002).

[3] K.I. Lee, Suk Wang Yoon, Feasibility of bone assessment with leaky {L}amb waves in bone phantoms and a bovine tibia, J. Acoust. Soc. Am. 115 (6) (2004) 3210–3217.

[4] G. Rizzuti, A. Gisolf, 2-D wavefield inversion for high-resolution elastic property estimation, in: 76th European Association of Geoscientists and Engineers Conference and Exhibition 2014: Experience the Energy - Incorporating SPE EUROPEC 2014, 2014, pp. 4606–4610.

[5] Pengfei Song, Xiaojun Bi, Daniel C. Mellema, Armando Manduca, Matthew W. Urban, James F. Greenleaf, Shigao Chen, Quantitative assessment of left ventricular diastolic stiffness using cardiac shear wave elastography, J. Ultrasound Med. 35 (7) (2016) 1419–1427.

[6] M.A. Fakih, S. Mustapha, J. Tarraf, G. Ayoub, R. Hamade, Detection and assessment of flaws in friction stir welded metallic plates, in: Proceedings of SPIE - the International Society for Optical Engineering, Vol. 10168, 2017.

[7] Zhongtao Hu, Zhiwu An, Yuanyuan Kong, Guoxuan Lian, Xiaomin Wang, The nonlinear S 0 lamb mode in a plate with a linearly-varying thickness, Ultrasonics 94 (2019).

[8] Mutsuki Matsushita, Naoki Mori, Shiro Biwa, Transmission of lamb waves across a partially closed crack: Numerical analysis and experiment, Ultrasonics 92 (2019).

[9] S. Otsuka, X. Shan, K. Yoshida, T. Yakura, M. Naito, Y. Kawakami, Site dependent elastic property of human iliotibial band and the effect of hip and knee joint angle configuration, J. Biomech. 109 (2020).

[10] H. Lamb, On waves in an elastic plate, Proc. R. Soc. A Math. Phys. Eng. Sci. 93 (648) (1917) 114–128.

[11] J.L. Rose, Ultrasonic Guided Waves in Solid Media, Vol. 9781107048, 2014, pp. 1–512.

[12] K.S. Tan, N. Guo, B.S. Wong, C.G. Tui, Experimental evaluation of delaminations in composite plates by the use of lamb waves, Compos. Sci. Technol. 53 (1) (1995).

[13] S.G. Pierce, B. Culshaw, W.R. Philp, F. Lecuyer, R. Farlow, Broadband lamb wave measurements in aluminium and carbon/glass fibre reinforced composite materials using non-contacting laser generation and detection, Ultrasonics 35 (2) (1997).

[14] Shen Wang, Songling Huang, Wei Zhao, Simulation of Lamb wave's interactions with transverse internal defects in an elastic plate, Ultrasonics 51 (4) (2011).

[15] Taoufiq Belhoussine Drissi, Bruno Morvan, Mihai Predoi, Jean Louis Izbicki, Pascal Pareige, Study of the transmission of ultrasonic guided wave at the junction of two different elastic plates with the presence of a defect, Key Eng. Mater. 482 (2011).

[16] Peter McKeon, Slah Yaacoubi, Nico F. Declercq, Salah Ramadan, Weina K. Yaacoubi, Baseline subtraction technique in the frequency-wavenumber domain for high sensitivity damage detection, Ultrasonics 54 (2) (2014) 592–603.

[17] E.V. Glushkov, N.V. Glushkova, A.A. Eremin, Guided wave based nondestructive testing and evaluation of effective elastic moduli of layered composite materials, Mater. Phys. Mech. 23 (1) (2015).

[18] Andrea Gianneo, Michele Carboni, Marco Giglio, Feasibility study of a multi-parameter probability of detection formulation for a lamb waves–based structural health monitoring approach to light alloy aeronautical plates, Struct. Health Monit. 16 (2) (2017).

[19] Wentao Wang, Yuequan Bao, Wensong Zhou, Hui Li, Sparse representation for lamb-wave-based damage detection using a dictionary algorithm, Ultrasonics 87 (2018).

[20] Pierre Kauffmann, Marie-Aude Ploix, Jean-François Chaix, Catherine Potel, Cécile Gueudre, Gilles Corneloup, François Baque, Multi-modal leaky lamb waves in two parallel and immersed plates: Theoretical considerations, simulations, and measurements, J. Acoust. Soc. Am. 145 (2) (2019).

[21] Elira Maksuti, Fabiano Bini, Stefano Fiorentini, Giulia Blasi, Matthew W. Urban, Franco Marinozzi, Matilda Larsson, Influence of wall thickness and diameter on arterial shear wave elastography: A phantom and finite element study, Phys. Med. Biol. 62 (7) (2017).

[22] Annette Caenen, Mathieu Pernot, Darya Alexandrovna Shcherbakova, Luc Mertens, Mathias Kersemans, Patrick Segers, Abigail Swillens, Investigating shear wave physics in a generic pediatric left ventricular model via <italic>in vitro</italic> experiments and finite element simulations, IEEE Trans. Ultrason. Ferroelectr. Freq. Control 64 (2) (2017) 349–361.

[23] Ivan Z. Nenadic, Matthew W. Urban, Scott A. Mitchell, James F. Greenleaf, Lamb wave dispersion ultrasound vibrometry (LDUV) method for quantifying mechanical properties of viscoelastic solids, Phys. Med. Biol. 56 (7) (2011) 2245–2264.

[24] Miguel Bernal, Ivan Nenadic, Matthew W. Urban, James F. Greenleaf, Material property estimation for tubes and arteries using ultrasound radiation force and analysis of propagating modes, J. Acoust. Soc. Am. 129 (3) (2011) 1344–1354.

[25] Clemens Grünsteidl, Todd W. Murray, Thomas Berer, István A. Veres, Inverse characterization of plates using zero group velocity lamb modes, Ultrasonics 65 (2016).

[26] Brennan Dubuc, A. Ebrahimkhanlou, Stylianos Livadiotis, Salvatore Salamone, Inversion algorithm for lamb-wave-based depth characterization of acoustic emission sources in plate-like structures, Ultrasonics 99 (2019).

[27] T.N.H.T. Tran, M.D. Sacchi, D. Ta, V.-H. Nguyen, E. Lou, L.H. Le, Nonlinear inversion of ultrasonic dispersion curves for cortical bone thickness and elastic velocities, Ann. Biomed. Eng. 47 (11) (2019) 2178–2187.

[28] Clemens Grünsteidl, Thomas Berer, Mike Hettich, István Veres, Using zero-group-velocity lamb waves to determine thickness and bulk sound velocities of isotropic plates, AIP Conf. Proc. 2102 (2019) 050016.

[29] Liqiang Zhu, Xiangyu Duan, Zujun Yu, On the identification of elastic moduli of in-service rail by ultrasonic guided waves, Sensors 20 (6) (2020) 1769.

[30] Matteo Mazzotti, Christopher Sugino, Eetu Kohtanen, Alper Erturk, Massimo Ruzzene, Experimental identification of high order lamb waves and estimation of the mechanical properties of a dry human skull, Ultrasonics 113 (2021) 106343.

[31] Yung-Chun Lee, Sheng-Wen Cheng, Measuring {L}amb wave dispersion curves of a bi-layered plate and its application on material characterization of coating, IEEE Trans. Ultrason. Ferroelectr. Freq. Control 48 (3) (2001) 830–837.

[32] J. Luis Deán, Cristina Trillo, Ángel F. Doval, José L. Fernández, Determination of thickness and elastic constants of aluminum plates from full-field wavelength measurements of single-mode narrowband lamb waves, J. Acoust. Soc. Am. 124 (3) (2008) 1477–1489.

[33] M. Sale, P. Rizzo, A. Marzani, Semi-analytical formulation for the guided waves-based reconstruction of elastic moduli, Mech. Syst. Signal Process. 25 (6) (2011) 2241–2256.

[34] Josquin Foiret, Jean-Gabriel Minonzio, Christine Chappard, Maryline Talmant, Pascal Laugier, Combined estimation of thickness and velocities using ultrasound guided waves: A pioneering study on in vitro cortical bone samples, IEEE Trans. Ultrason. Ferroelectr. Freq. Control 61 (9) (2014) 1478–1488.

[35] Michael Ponschab, Daniel A. Kiefer, Stefan J. Rupitsch, Simulation-based characterization of mechanical parameters and thickness of homogeneous plates using guided waves, IEEE Trans. Ultrason. Ferroelectr. Freq. Control 66 (12) (2019) 1898–1905.

[36] Alexander Velichko, Paul D. Wilcox, Excitation and scattering of guided waves: Relationships between solutions for plates and pipes, J. Acoust. Soc. Am. 125 (6) (2009) 3623–3631.

[37] C.Y. Chang, F.G. Yuan, Dispersion curve extraction of lamb waves in metallic plates by matrix pencil method, in: Proceedings of SPIE - the International Society for Optical Engineering, Vol. 10168, 2017.

[38] P. Zabbal, G. Ribay, B. Chapuis, J. Jumel, Multichannel multiple signal classification for dispersion curves extraction of ultrasonic guided waves, J. Acoust. Soc. Am. 143 (2) (2018) EL87–EL92.